Chinese Chemical Letters 36 (2025) 109998

Contents lists available at ScienceDirect

Chinese Chemical Letters

journal homepage: www.elsevier.com/locate/cclet

Molecular-based porous polymers with precise sites for photoreduction of carbon dioxide

Wei-Jia Wang[a], Kaihong Chen[b,*]

[a] College of Biological and Chemical Engineering, Zhejiang University of Science and Technology, Hangzhou 310023, China
[b] The Institute of Green Chemistry and Engineering, School of Chemistry and Chemical Engineering, Nanjing University, Suzhou 215163, China

ARTICLE INFO

Article history:
Received 21 February 2024
Revised 13 March 2024
Accepted 10 May 2024
Available online 11 May 2024

Keywords:
Carbon dioxide reduction
Photocatalysis
Porous polymers
Well-defined catalytic sites
Molecular level

ABSTRACT

Photocatalytic CO_2 reduction reaction (CO_2RR) is one of the promising strategies for sustainably producing solar fuels. The precise identification of catalytic sites and the enhancement of photocatalytic CO_2 conversion is imperative yet quite challenging. This critical review summarizes recent advances in porous photo-responsive polymers, including covalent organic frameworks (COFs), covalent triazine frameworks (CTFs), and conjugated microporous polymers (CMPs), those can be rationally designed from the molecular level for visible-light-driven photocatalytic CO_2 reduction. Additionally, special emphasis is placed on how the well-defined active sites on these polymers can influence their properties and photocatalytic performance. The precise regulation and control of microenvironments and electronic properties of metal active centers are crucial for boosting catalytic efficiency and selectivity, as well as for the design of better photocatalysts for CO_2 reduction.

1. Introduction

With the increasing energy shortage and environmental problems, finding clean and renewable energy sources to replace fossil fuels has become an urgent task [1,2]. Large-scale deployment of artificial systems that mimic natural photosynthesis could accomplish solar energy storage, CO_2 sequestration, and recycling of carbon back into fuels for energy consumption, thereby relieving our dependency on fossil fuels [3-9]. In recent years, solar-driven photocatalytic CO_2 reduction reaction (CO_2RR) has attracted growing attention and is regarded as a renewable and sustainable strategy. The core of CO_2 photocatalytic technology lies in the development of photocatalysts that can absorb light and efficiently convert CO_2 into "solar fuels" including carbon monoxide (CO), formic acid (HCOOH), methanol (CH_3OH), methane (CH_4) and so on (Fig. 1) [10-17].

Photocatalytic CO_2 reduction reactions are complex multistep processes, and their efficiency is influenced by several factors (Fig. 2) [18-26]. Firstly, the critical starting step is the absorption of light with energy equal to or greater than the bandgap by semiconductor photocatalyst, which generates photogenerated electrons and holes. To maximize the utilization of solar energy, it is desirable to use photocatalysts that can absorb visible light. The band structure is also an important factor in determining whether the photocatalytic reduction of CO_2 can occur. To mimic natural photosynthesis, water should be used as the hole scavenger, meaning the bandgap of photocatalyst should straddle both the potentials for CO_2 reduction and water oxidation. Better separation of photogenerated electrons and holes can bring a higher surface photogenerated electron density in photocatalysts, which can effectively accelerate multi-electron reduction reaction. Additionally, surface catalytic active sites and/or cocatalysts can enhance separation of photogenerated carriers and promote surface redox reactions. The adsorption and desorption of reactants, intermediates, and products also play a key role in reaction efficiency and product selectivity. Strong adsorption ability of reactants and easy desorption of the target product can result in a high yield of the desired product.

Currently, significant progress has been made in the development of novel photoreduction CO_2 systems [27,28]. Particulate photocatalysts, including metal oxide, metal sulphide, metal (oxy)nitride, have demonstrated successful applications in photocatalytic CO_2RR [29-42]. However, this process is hindered by low charge separation and migration efficiency, inevitable electron-hole recombination, and the inert nature of CO_2 molecules [43,44]. As a result, the quantum yield and lifetime of photocatalysts are still far behind the need for practical applications. Compared with these photocatalysts, porous polymers (PPs) such as covalent organic frameworks (COFs), covalent triazine frameworks (CTFs), and conjugated microporous polymers (CMPs), offer the potential for

* Corresponding author.
E-mail address: kchen@nju.edu.cn (K. Chen).

https://doi.org/10.1016/j.cclet.2024.109998
1001-8417/

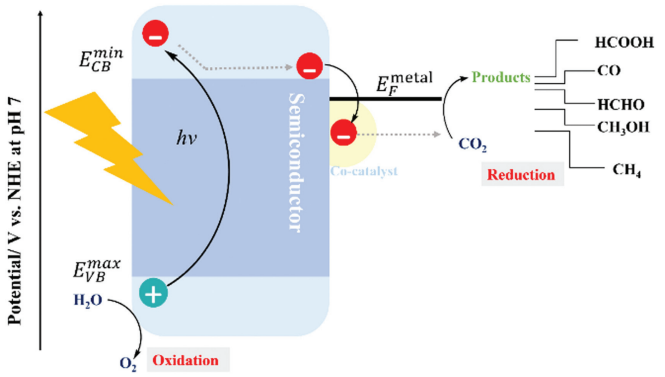

Fig. 1. CO_2RR to product solar fuel molecules and the reaction mechanism from semiconductor catalysts.

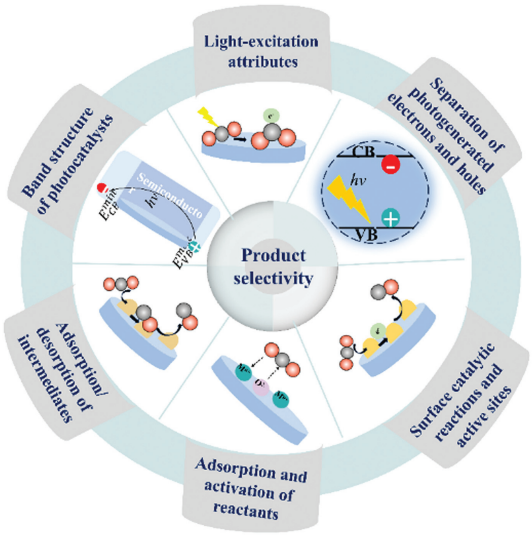

Fig. 2. Main factors influencing the product selectivity of photocatalytic CO_2 reduction reactions.

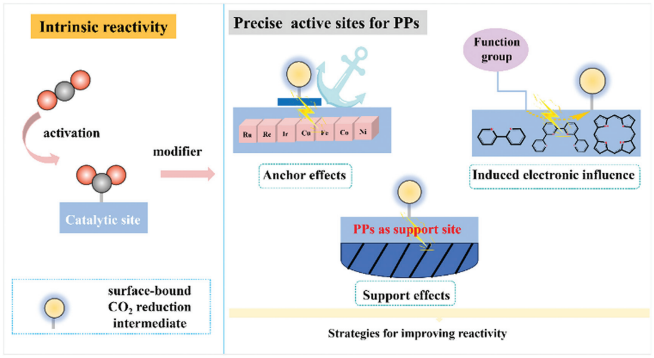

Fig. 3. Classification of precise active sites effects of PPs in photocatalytic CO_2RR for improving reaction reactivity.

higher CO_2RR efficiency while providing opportunities to explore the structure–property relationship at the molecular level [45-56]. Additionally, the large surface area of PPs facilitates mass transport and ion migration during the reaction. Due to the tunable structure and large surface area, PPs can also serve as supports to stabilize and synergistically enhance the activity of active sites.

In this review, we present a perspective on PPs with structurally well-defined active metal sites for CO_2 photocatalytic reduction (Fig. 3). We focus on gaining a deeper understanding of how well-defined active sites of PPs can influence optical properties, photo-generated charge separation and transport, and overall photocatalytic performance. Furthermore, this review aims to explore the multi-chemical microenvironment of PPs to improve performances, especially selectivity, and provide inspiration for novel tailored designs of future photocatalytic CO_2RR systems that are more efficient and stable. Ultimately, these advancements will drive innovations and commercialization in photocatalysis.

Table 1
Photocatalytic multielectron processes of CO_2RR [61,62].

Entry	Reaction	E_{red}[a] (V)
1	$2H^+ + 2e^- \rightarrow H_2$	−0.41
2	$CO_2 + 2H^+ + 2e^- \rightarrow HCOOH$	−0.61
3	$CO_2 + 2H^+ + 2e^- \rightarrow CO + H_2O$	−0.53
4	$CO_2 + 4H^+ + 4e^- \rightarrow HCHO + H_2O$	−0.48
5	$CO_2 + 6H^+ + 6e^- \rightarrow CH_3OH + 2H_2O$	−0.38
6	$CO_2 + 8H^+ + 8e^- \rightarrow CH_4 + H_2O$	−0.24
7	$2H_2O \rightarrow O_2 + 4H^+ + 4e^-$	+0.81

[a] redox potentials are referred to NHE at pH 7.

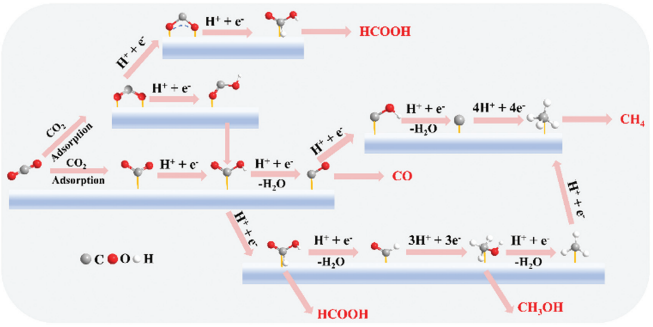

Fig. 4. Proposed reaction paths for PPs photocatalytic CO_2RR.

2. Superiority of PPs in photocatalytic CO_2RR

2.1. Effective CO_2 activation

CO_2 is an exceptionally stable molecule due to the high C=O bonding energy (750 kJ/mol) [50]. Consequently, a substantial negative reduction potential of −1.9 V (*vs.* NHE) is required for the one-electron reduction of CO_2 to generate $CO_2^{\bullet-}$ [57]. Additionally, the kinetic inertness of CO_2, originating from its poor solubility in solvents and the multi-step process involving electron and proton transfer (Table 1 and Fig. 4), presents a bottleneck for CO_2RR. Moreover, the presence of side reactions, such as H_2 evolution reaction, can hinder the efficient utilization of photons for the desired product. To address these issues, one potential solution is to create CO_2 activation sites on photocatalysts.

PPs have been recognized as ideal CO_2 adsorbents that can adsorb CO_2 and then activate it. Increasing the BET specific surface area and microporosity of PPs is one of commonly used approach to enhance CO_2 adsorption capacity [58]. Modifying the surface structure of photocatalyst also proves to be an effective means to provide the active sites for CO_2 adsorption. Three primary strategies have been developed in this regard, *i.e.*, heteroatoms doping, defect engineering, and introducing CO_2-philic groups to enhance the adsorption [59,60].

2.2. Tunable band structures

Upon the absorption of a photon with energy equal to or higher than the band gap, an electron is excited from the valence band maximum (VBM) to the conduction band minimum (CBM), leaving behind a hole as a quasiparticle [61-66]. Once spatially separated,

these carriers can migrate to the surface for redox reactions [59]. To maximize light utilization, a smaller band gap will be highly desirable. Additionally, the band structure should straddle the potentials associated with CO_2RR and oxygen evolution reaction (OER), when using water as the hole scavenger [67-74]. Screening photocatalysts with suitable band structures can be a time-consuming work. However, PPs provide a promising solution to this challenge as the band structure can be easily adjusted by varying the starting materials.

2.3. Designable metal supporter

Cocatalysts play a crucial role in photocatalysis as they facilitate charge separation/transport and catalyze surface redox reactions [75-77]. Furthermore, the complicate reaction process (Table 1) often leads to low product selectivity, which can be alleviated by the presence of a highly selective active center. Different metals lead to various kinetic and thermodynamic properties, thereby influencing the reaction pathway and the types of products. PPs, with their well-defined coordination environment and enhanced metal-support interactions, demonstrate remarkable catalytic performance in heterogeneous reactions [78-81]. Recent advancements in the implementation of molecular-based design for CO_2 reduction have proven highlighted the importance of microenvironments and electronic properties of single-metal sites active centers in determining catalytic activity and selectivity [82-85]. PPs containing catalytically active metal centers enable precise control over atomic configuration. These designed PP materials allow fine-tuning of chelating abilities and steric effects of ligands, thereby facilitating accurate modulation of the local coordination environment and electronic properties of active centers. In addition, such metal cocatalyst possess unfilled d orbitals, making them highly receptive to CO_2 adsorption and capable of forming intermediates with anchor effects at active sites.

2.4. High stability in photocatalytic CO_2RR

The stability of catalyst is a critical parameter in photocatalytic CO_2RR, as it determines the practical applicability of the catalyst [86]. The stability of PPs catalytic systems can be divided into two aspects: the stability of active sites and the stability of the PPs skeleton. During the catalytic reaction, active sites may aggregate or become poisoned, resulting in inactivity, and the skeleton may undergo collapse or breakage, resulting in reduced catalytic efficiency of the overall system [87]. To address these challenges, robust PPs skeletons, such as CTFs and olefin-linked COFs, have been developed and explored the inactivation mechanism [88].

3. Application of porous polymer based catalysts in photocatalytic CO_2 reduction reaction

3.1. Photocatalytic CO_2RR by COF based catalysis

In 2005, Yaghi *et al.* discovered COFs, which provided hope for effective photocatalysts [89]. COFs are composed of various organic molecular building blocks that are ordered periodically through covalent bonds. These bonds include imine, triazine, β-ketoenamine, hydrazone, olefin, azine, and others [90]. The structural features of COF offer numerous advantages, such as suitable energy band structures, designability of periodic structures, high surface area, reactant accessibility, and low density. Given these inherent advantages and the potential impact on the global energy crisis [91-96], two main methods are used to develop a well-designed plan to further developing efficient system (Fig. 5).

Compared to other photocatalysts, COFs can combine porosity with crystallinity to stabilize intermediates for photocatalytic

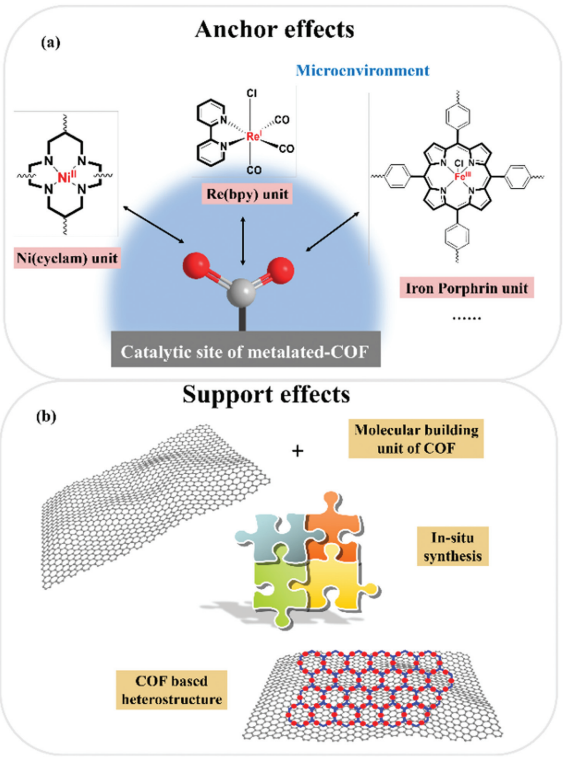

Fig. 5. The effect of COF based catalysis for photocatalytic CO_2RR. (a) Anchor effect on metalated-COF. (b) Support effect on COF based heterostructure.

CO_2RR. For example, an azine-based COF, N_3-COF, was shown to exhibit gas phase photocatalytic CO_2 reduction ability [97]. However, several challenges remain, including limited visible-light harvesting ability, poor selectivity, and difficulty in separating photogenerated electron–hole pairs [98-103]. In this regard, particular attention is warranted in regulating the coordination spheres in single COF catalysts and fabricating COF heterojunctions to address these pressing challenges in CO_2RR.

COFs represent a wide class of materials that can alter the chemical environment through anchoring different types of metals and ligands for CO_2RR catalysis. The photosensitive metal sites in COFs can transport photogenerated electrons, which typically act as active sites for initiating photocatalysis. This feature ensures high electron−hole separation and promotes high activity in photocatalysis. In a recent study by Huang *et al.*, they reported a newly designed 2D COF incorporating a Re complex, which exhibited intrinsic light absorption and charge separation properties (Fig. 6a) [103]. This hybrid catalyst efficiently reduced CO_2 to CO under visible light illumination with higher selectivity (98%) and activity than its homogeneous Re counterpart. More importantly, through advanced transient optical and X-ray absorption spectroscopy, as well as *in situ* diffuse reflectance spectroscopy, they unraveled three key intermediates (Re-COF$^-$, TEOA$^+$-Re-COF$^-$, Re-COF-CO_2 adduct) that are responsible for charge separation, the induction period, and rate limiting step in catalysis. This work not only demonstrates the potential of COFs as next generation photocatalysts for solar fuel conversion, but also provides unprecedented insight into the mechanistic origins of high product selectivity in light-driven CO_2 reduction.

In addition, Cooper's group demonstrated that tethering a rhenium complex, [Re(bpy)$(CO)_3$Cl], into a COF structure, results in a heterogeneous photocatalyst with a strong visible light absorption, high CO_2 binding affinity, and improved catalytic performance compared to its homogeneous counterpart (Fig. 6b) [104]. This COF

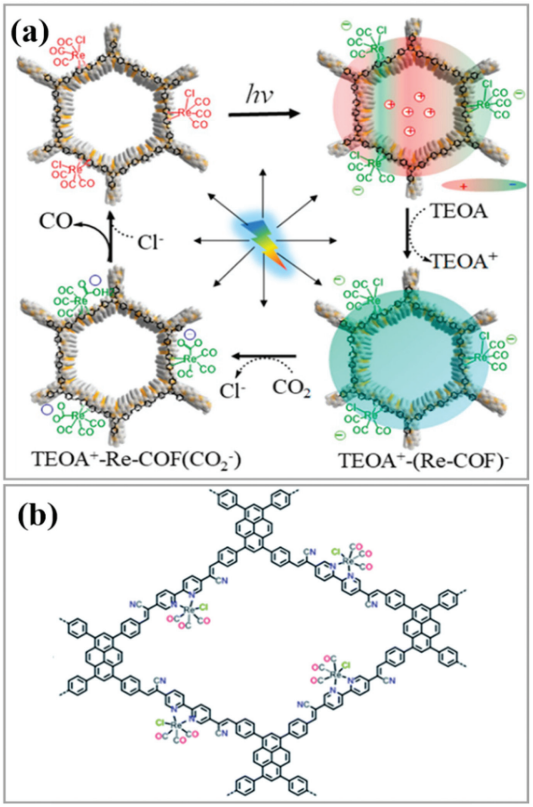

Fig. 6. Photosensitive metal Re site in COFs for PCO_2RR. (a) The structure of 2D Re-COF Copied with permission [103]. Copyright 2018, American Chemical Society. (b) The structure of 2D bipyridine-containing COF with Re site. Copied with permission [104]. Copyright 2020, the Royal Society of Chemistry.

incorporates bipyridine sites, which allow for the ligation of the Re complex, into a π-conjugated backbone that is chemically robust and promotes light-harvesting.

Another promising approach involves incorporating molecular catalytic components into the intrinsic pores of COFs, enabling the resultant composites to possess advantages of both homogeneous and heterogeneous catalysts. However, the binding ability of bipyridyl unit in COFs is not strong enough to stabilize active metal centers, leading to unavoidable metal leaching during CO_2 reduction, even in the presence of excess bipyridyl units [105,106]. Porphyrin units, with stronger chelating coordination ability towards metal ions, offer a promising alternatives [107,108]. Consequently, metalloporphyrin-based COFs have been developed by introducing porphyrin units into the host frameworks. Ultrathin Co-porphyrin-based COF nanosheets and corresponding bulk materials show high durability and cyclability in visible-light-driven CO_2-to-CO conversion [109]. Lan *et al.* demonstrated that crystalline porphyrin-tetrathiafulvalene COFs can serve as photocatalysts for reducing CO_2 with H_2O (Fig. 7a) [110]. Effective transfer of photogenerated electrons from tetrathiafulvalene to porphyrin *via* covalent bonding allows for separated electrons and holes for CO_2 reduction and H_2O oxidation, respectively. Tuning the metal ion of COF, these TTCOFs exhibited a broad visible-light absorption range, and the corresponding band gaps (E_g) were determined to be 1.15, 1.49, 1.33, and 1.39 eV for TTCOF-2H/Zn/Ni/Cu by Tauc plots, respectively. By adjusting the band structures of TTCOFs, TTCOF-Zn achieved higher CO evolution of 12.33 μmol under visible light illumination after 60 h than that of TTCOF-Cu (8.65 μmol) and TTCOF-Ni (0.462 μmol) with almost 100% selectivity, accompanied by H_2O oxidation to O_2 (Figs. 7b and c). In Jiang's work, by fine-tuning the inter-layer spacing of porphyrin-based 2D COFs (Fig. 8a) [111],

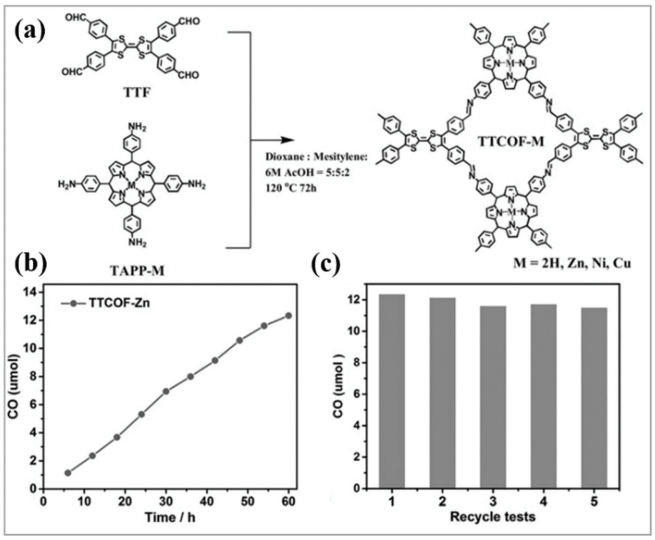

Fig. 7. (a) The synthesis of TTCOF-M and (b, c) photocatalyst CO_2RR performance. Copied with permission [110]. Copyright 2019, Wiley-VCH.

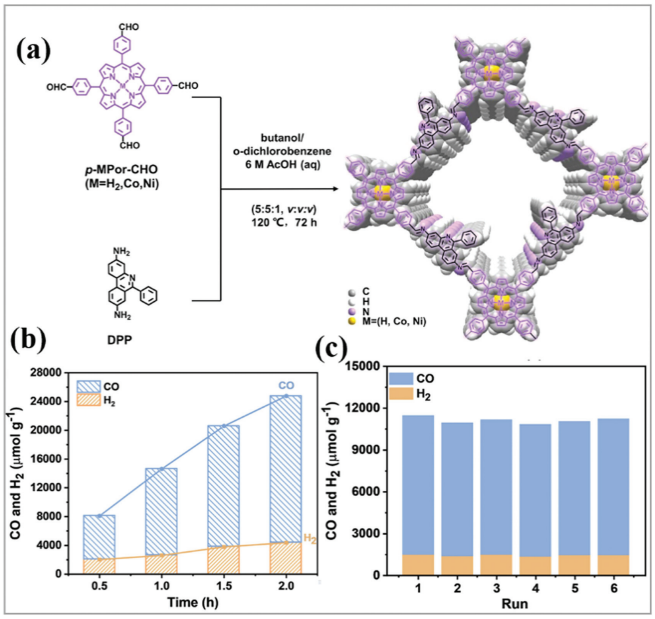

Fig. 8. (a) The synthesis of MPor-DPP-COF and (b, c) photocatalyst CO_2RR performance. Copied with permission [111]. Copyright 2022, American Chemical Society.

MPor-DPPCOFs, showed excellent photocatalytic activity for CO_2RR, with a CO generation rate of 10,200 μmol g^{-1} h^{-1} and a CO selectivity up to 82% (Figs. 8b and c).

Considering the unambiguous structures, high density of catalytic sites, and strong conjugation ability of metalloporphyrin-based COFs [112,113], exploiting isostructural platforms based on them can offer valuable insights into the chemical interactions between metal active sites and the reagents/reactive intermediates during CO_2 photoreduction. However, the activities of pristine COFs are still unsatisfactory partly due to photogenerated carriers easily recombination. To enhance the solar-to-fuel conversion efficiency, COF-based heterostructures combining COFs with metal-sulfides [114-119], metal-oxides [120-122], carbon materials [123,124], or MOFs [125,126], have gained increasing attention. These heterostructures facilitate interfacial photo-generated carrier separation and promote surface redox reactions. In Lan's work, "all solid states direct Z-Scheme heterostructure" has been proposed

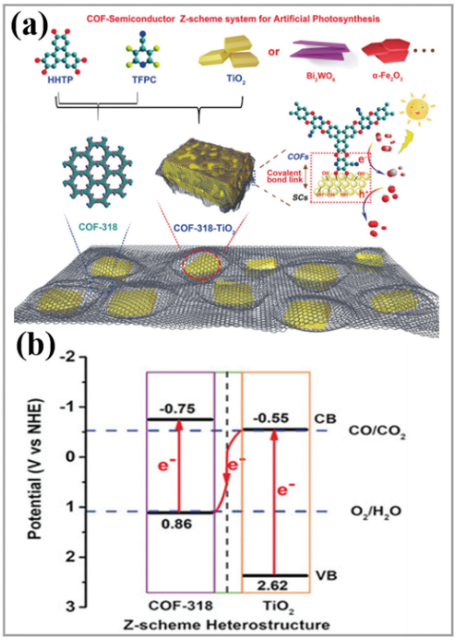

Fig. 9. (a) COF-semiconductor Z-scheme system for artificial photosynthesis. (b) The charge-transfer process under light irradiation with the Z-scheme model. Copied with permission [113]. Copyright 2020, Wiley-VCH.

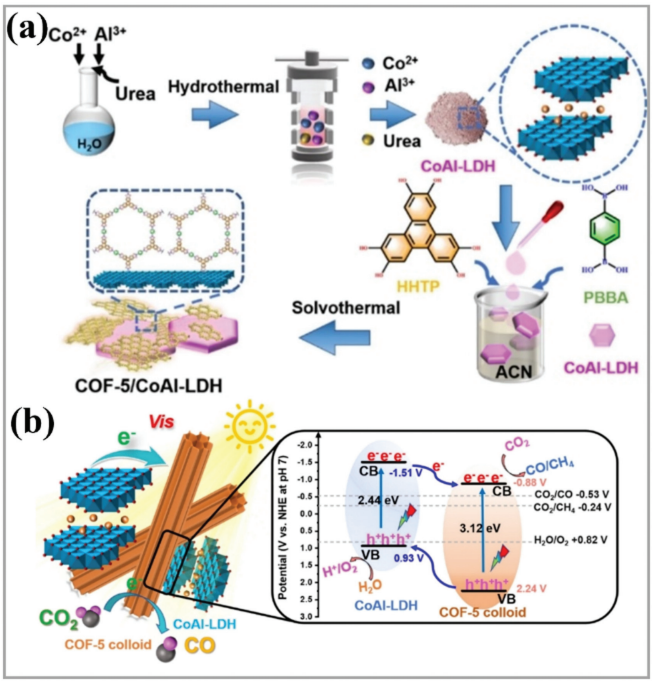

Fig. 10. (a) The synthesis of COF-5/CoAl-LDH nanocomposite and (b) proposed mechanism. Copied with permission [128]. Copyright 2022, Wiley-VCH.

for photocatalytic CO_2RR, COF-semiconductor Z-scheme photocatalysts combining COFs (COF-316/318) with water-oxidation semiconductors (TiO_2, Bi_2WO_6, and α-Fe_2O_3) were synthesized, exhibiting high CO_2-to-CO conversion efficiencies (up to 69.67 μmol g^{-1} h^{-1}) using H_2O as the only electron donor, without the need for additional photosensitizers or sacrificial agents (Fig. 9a) [113]. This marks the first report of covalently bonded COF/inorganic-semiconductor systems utilizing the Z-scheme for artificial photosynthesis. The key to achieving successful integration lies in the effective transfer of charge carriers between the semiconductor and the COF (Fig. 9b). Furthermore, specific active sites for CO_2 reduction in the COF, such as pyridine (site-N) and cyano group (site-CN), were considered [113,127]. The pyridine group facilitates the first step of CO_2 activation, then the cyano group promotes the proton-coupled electron-transfer process (*COO-*CO). The combination of pyridine and cyano groups leads to higher CO_2 reduction activity.

As discussed above, the interactions between the photocatalyst and CO_2 play a crucial role in subsequent photocatalytic reduction. Herein, Liu *et al.* reported the 1D/2D heterojunction (COF-5/CoAl-LDH) by direct *in-situ* synthesis of the COF-5 colloid on the surface of CoAl layered double hydroxide (LDH) was used as the prospective photocatalyst for CO_2 reduction (Fig. 10a) [128]. The CoAl-LDH is rich in metal atoms coordinated by six-fold hydroxyl groups, providing favorable adsorption of CO_2 and stabilization of the intermediate COOH*. The band structure of COF and LDH contributes to a type II heterostructure, inhibiting the recombination of carriers generated by photon absorption of COF (Fig. 10b). Through the synergistic effect of promoted CO_2 adsorption and enhanced charge separation, the optimal COF-5/CoAL-LDH heterostructure achieved a CO generation selectivity of 96.4% and a CO generation rate of 53 μmol g^{-1} h^{-1}.

The introduction of molecular catalytic components into the internal cavities of COFs is a promising method that combines the advantages of homogeneous and heterogeneous catalysts [129-133]. In the work of Wang *et al.,* carbon quantum dots were prepared from the pyrolysis of metalloporphyrin (M-PCD) and immobilized in the pores of as-synthesized TD COF *via* sonication and

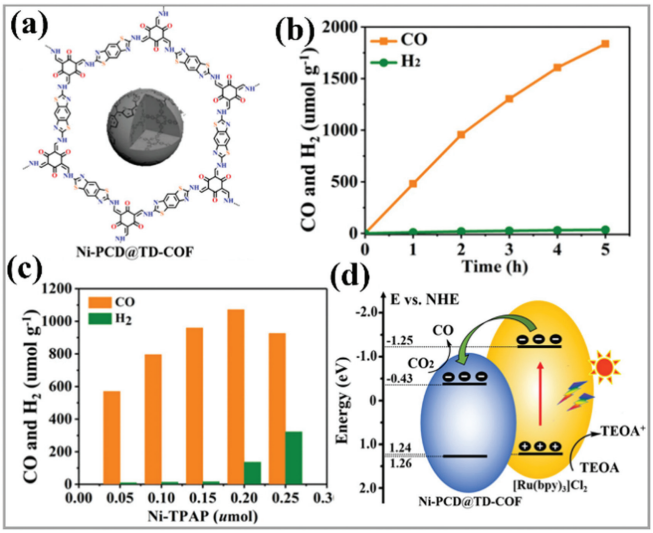

Fig. 11. (a) The structure of TD-COF and Ni-PCD@TD-COF. (b, c) The CO_2RR performance of Ni-TPAP. (d) The energy-level diagram showing the electron transfer from $[Ru(bpy)_3]Cl_2$ to Ni-PCD@TD-COF. Copied with permission [134]. Copyright 2020, Wiley-VCH.

thermal treatment under N_2 (Fig. 11a) [134]. This configuration enables the adsorption of CO_2 and prevents the leaching of the carbon quantum dots. The resulting M-PCD@TD-COF heterostructure exhibits a CO evolution rate of 578 μmol h^{-1} g^{-1} with 98% selectivity towards CO under visible light irradiation, further enhanced by $[Ru(bpy)_3]^{2+}$(Figs. 11b and c). The corresponding energy level diagram is shown in Fig. 11d. The conduction band of Ni-PCD@TD-COF is lower than the LUMO of $[Ru(bpy)_3]Cl_2$, so that the photoexcited electrons in the LUMO of photosensitizers could transfer to the CBM of Ni-PCD@TD-COF, enabling the reduction of adsorbed CO_2 to generate CO. Another COF-based heterostructure was fabricated by Do *et al.,* where they synthesized TpPa-1 COF on graphene oxide (GO) and then reduced GO to reduced graphene oxide (rGO)

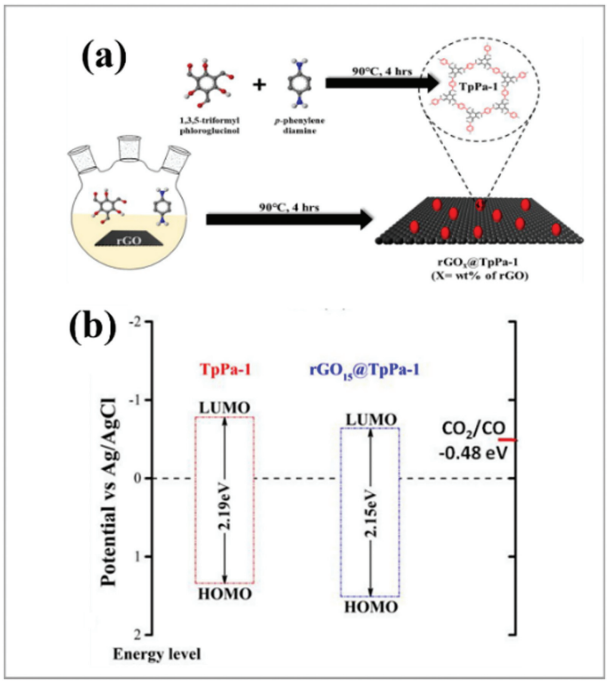

Fig. 12. (a) The *in situ* process for the synthesis of covalently bonded rGOx@TpPa-1 composites. (b) The energy level diagram of TpPa-1 and rGOx@TpPa-1. Copied with permission [135]. Copyright 2021, American Chemical Society.

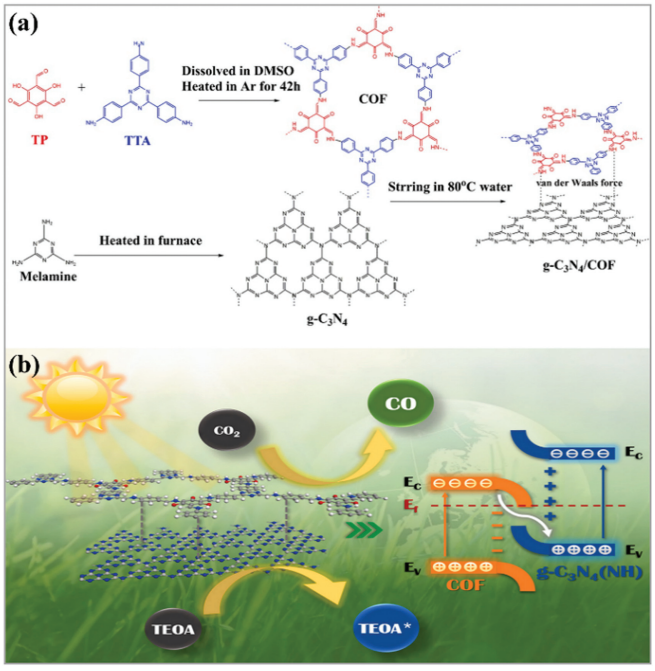

Fig. 13. (a) The preparation of g-C_3N_4/COF heterojunction. (b) The relative band energy positions and S-scheme charge transfer mechanism between Tp-Tta COF and g-C_3N_4. Copied with permission [136]. Copyright 2022, Elsevier B.V.

in situ (Fig. 12a) [135]. The inclusion of rGO promotes the effective utilization of photo-generated carriers and increases the absorption of visible light (Fig. 12b). This optimized COF/rGO photocatalyst achieved a CO evolution rate of 200 μmol h^{-1} g^{-1} with 89% selectivity towards CO under visible light irradiation. Defective g-C_3N_4 can also form a heterostructure with COF for photocatalytic CO_2RR, as discovered by Ye *et al.* (Fig. 13a) [136]. In this work, N-vacancies in g-C_3N_4 increase the Fermi level difference between

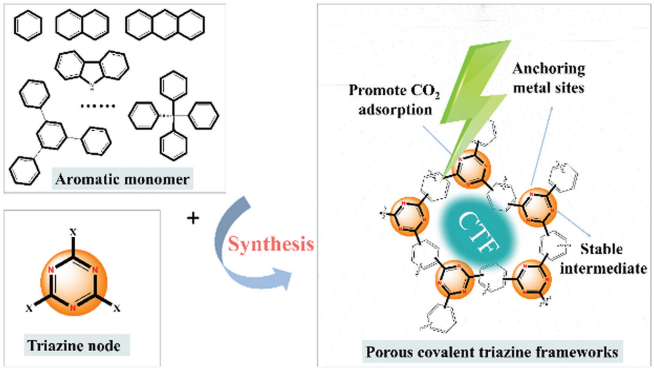

Fig. 14. CTFs *via* synthesis methods that use varying aromatic and cyanuric halides as monomers.

the TP-TTA COF and g-C_3N_4 facilitating charge transfer (Fig. 13b). This leads to a CO production rate of 576 μmol h^{-1} g^{-1} with 90.4% selectivity towards CO under visible light irradiation.

More recently, Zhou *et al.* studied a series of COF-organic molecular heterostructures as effective photocatalysts for CO_2RR [137]. Anthracene, pyrene, and perylene were assembled on TM-Ben COF (olefin-linked COFs named as TMBen) *via* an end-capping strategy. The formation of covalent bond facilitates charge separation through a Type II pathway and minimized charge recombination. Among them, the TMBen-Perylene heterostructure showed the highest CO_2RR activity with a rate of 93.0 μmol h^{-1} g^{-1} under visible light irradiation, using TEOA as the hole sacrificial agent. The brief summary of the photocatalytic performances of the COF-based photocatalysts in CO_2RR are listed in Table 2 [103-106,108,109,113,114,138-141].

3.2. Photocatalytic CO_2RR by CTF based catalysis

Two dimensional crystalline CTFs consist of covalently bonded aromatic triazines and exhibit unique structural characteristics, such as strong conjugated structure, delocalized electrons, and abundant active centers. These characteristics make CTFs highly promising in energy storage and conversion applications. In particular, CTFs are considered ideal photocatalysts for CO_2 reduction because of the strong interaction between N atoms in triazine cores and CO_2 [142,143]. This interaction, known as dipole or quadrupole interactions, dramatically reduces the energy barrier for CO_2 reduction, facilitating electron acceptance and subsequent reduction. One of the advantages of CTFs as photocatalytic systems is the synergic coordination between triazine units and nanoparticles or metal ions, as well as the confinement effect of the frameworks. This makes CTFs an attractive platform for immobilization metal nanoparticles [144-147]. To enhance photocatalytic efficiency and selectivity, co-catalysts (metal complexes), have been widely incorporated into CTFs frameworks to reduce overpotential, promote transfer kinetics, and enhance interfacial interactions during catalytic processes, leading to higher selectivity and efficiency in specific products formation [148]. Therefore, CTFs can serve as carriers for anchoring metal single atoms and assembling molecular-based complex for photocatalytic CO_2 reduction (Fig. 14) [148-157].

Maximizing atom-utilization efficiency on CTFs is crucial for facilitating charge separation and CO_2 activation in photocatalytic CO_2 reduction. Using suitable supports with strong interactions with the single atoms can help maintain the single-atom state of metal atoms. Moreover, the metal-support interaction can modify the electronic structure of the confined single atoms, influencing CO_2 capture and activation in metal centers. Recently, Wu's group reported a well-defined positioned synthesis of Pt single atoms in ethylene glycol (EG)-modified CTF (Pt-SA/CTF-1) using a

Table 2
Summary of photocatalytic CO_2 reduction using COF based photocatalysts.

Catalysts	Additive	Time (h)	Products (μmol g^{-1} h^{-1})[a]	Selectivity (%)	Ref.
Re-COF	$Re(bpy)(CO)_3Cl$/TEOA	20	CO:750	98	[103]
Re-Bpy-sp^2-c-COF	TEOA	17.5	CO:1040	81	[104]
Re-Bpy-sp^2-c-COF	$(Ir[dF(CF_3)ppy]_2(dtbpy))PF_6$/ TEOA	5	CO:1400	86	[104]
Ni-TpBpy-COFs	$Ru(bpy)_3Cl_2$/TEOA	5	CO:811.4	96	[105]
DQTP-COF-Co	$Ru(bpy)_3Cl_2$/TEOA	4	CO:1020	59.4	[106]
DQTP-COF-Zn	$Ru(bpy)_3Cl_2$/TEOA	4	HCOOH:152.5	90	[106]
TTCOF-Zn	–	60	CO:2.06	100	[108]
N_3–COF	–	24	CH_3OH:0.57	~100	[109]
ACOF-1	–	24	CH_3OH:0.36	~100	[109]
COF-318-TiO_2	–	4	CO:69.67	–	[113]
COF-367-Co NS	$Ru(bpy)_3Cl_2$/ascorbic acid	2	CO:10,162	78	[114]
CuO_2/WO_2–001	–	24	CO:5.73	65	[138]
NH_2–MIL-125(Ti)	–	10	HCOOH:16.3	100	[139]
NH_2-UiO-66(Zr)	–	10	HCOOH:26.4	100	[140]
Pt/NH_2–MIL-125(Ti)	–	8	HCOOH:25.9	100	[141]

[a] Maximum CO_2RR yield. TEOA: triethylamine.

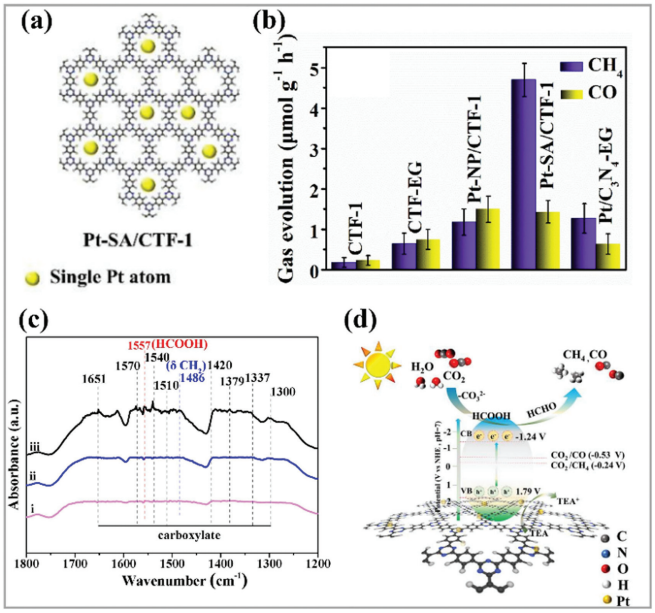

Fig. 15. (a) The structure of Pt-SAC/CTF-1. (b) Photocatalytic CO_2 conversion rates of CTF-1, CTF-EG, Pt-NP/CTF-1, Pt-SA/CTF-1 and Pt/C_3N_4-EG. (c) *In-situ* FTIR spectra of the adsorbed species for Pt-SA/CTF-1. (d) The mechanization of photocatalytic CO_2 reduction for Pt-SA/CTF-1. Copied with permission [158]. Copyright 2022, Elsevier B.V.

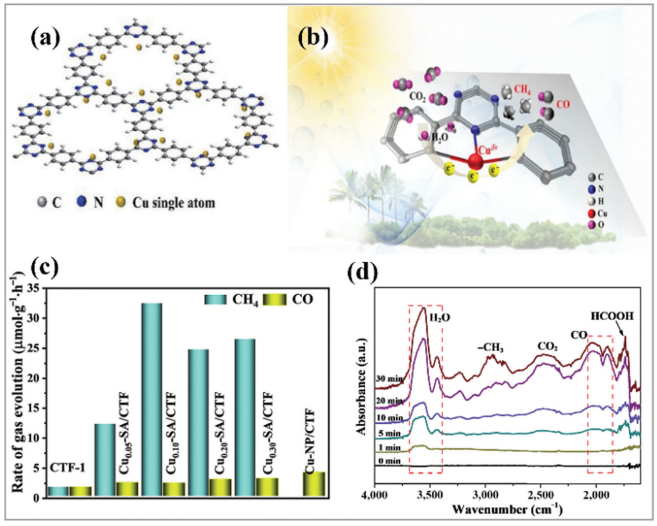

Fig. 16. (a) The structure of Cu-SA/CTF. (b) Photocatalytic CO_2 reduction performance of CTF-1, Cu-NP/CTF, and Cux-SA/CTF. (c) *In-situ* FTIR spectra of the adsorbed species for Cu0.10-SA/CTF. (d) The conversion of photocatalytic CO_2 reduction for Cux-SA/CTF. Copied with permission [159]. Copyright 2022, Springer.

photo-deposition method for efficient photoreduction CO_2 to CH_4 under visible light irradiation [158]. The well-defined coordination structure of Pt–N(C) sites in the Pt-SA/CTF-1 catalyst demonstrates that Pt single atoms confined in CTF-1 not only improve CO_2 adsorption and activation but also accelerate the separation and transfer of photogenerated carriers in CTF-1 (Fig. 15a). When exposed to visible light, Pt-SA/CTF-1 is excited, generating electron and hole pairs. The photogenerated electrons are then transferred to the single Pt atoms, while the holes are quenched by TEA. With a continuous supply of electrons, the adsorbed CO_2 are activated to formed carbonate ($-CO_3^{2-}$); which are subsequently reduced to intermediates such as HCOOH and HCHO, and finally transformed into CH_4, as the main reduction product (Figs. 15b and c). The high affinity of Pt-SA/CTF-1 for CO_2 also played a crucial role in promoting the formation of Pt-CO_2 adduct and consequently boosts the performance of photocatalytic CO_2 reduction (Fig. 15d).

Similarly, Zhang's group has successfully designed and synthesized photocatalysts using CTFs anchored with copper single atoms (Cu-SA/CTF) to enhance the conversion of CO_2 (Fig. 16a) [159]. These Cu-SA/CTF photocatalysts exhibit superior performance with a high selectivity of 98% in the photocatalytic CO_2 conversion to CH_4 (Fig. 16b). The introduction of Cu single atoms enhances CO_2 adsorption capacity, visible light absorption ability, and separation efficiency of photogenerated carriers, ultimately improving the photocatalytic activity. The photocatalytic pathway of Cu-SA/CTF involves the adsorption of *CO, and *HO intermediates. Subsequently, the adsorbed *CO can react with protons and electrons to produce COOH*. Then, COOH* species could be further protonated into CHOH or CH_4. The desorption of CO was obtained *via* the dissociation of OH from COOH* (Figs. 16c and d). In brief, the photocatalytic conversation process is described as CO_2 to CH_4. It demonstrated that constructing excellent molecular-based CTFs endows their high selective for photocatalysis CO_2RR.

In Cao's work, a pyridine-based CTF (CTF-py) derived from 2,6-dicyanopyridine is employed as a porous platform to anchor the Re carbonyl complex $Re(CO)_3Cl$ (Re-CTF-py). The resulting Re-CTF-py photocatalyst demonstrates high efficiency in photocatalytic CO_2 reduction to CO, achieving a turnover number (TON) of 4.8. The CO evolution rate reached 353.05 μmol g^{-1} h^{-1} within 10 h under full light irradiation in a solid-gas system. Moreover, the single-site Re-CTF-py catalyst prevents the dimerization and leaching of active Re species, ensuring sustained activity [160]. Single-site catalysts with

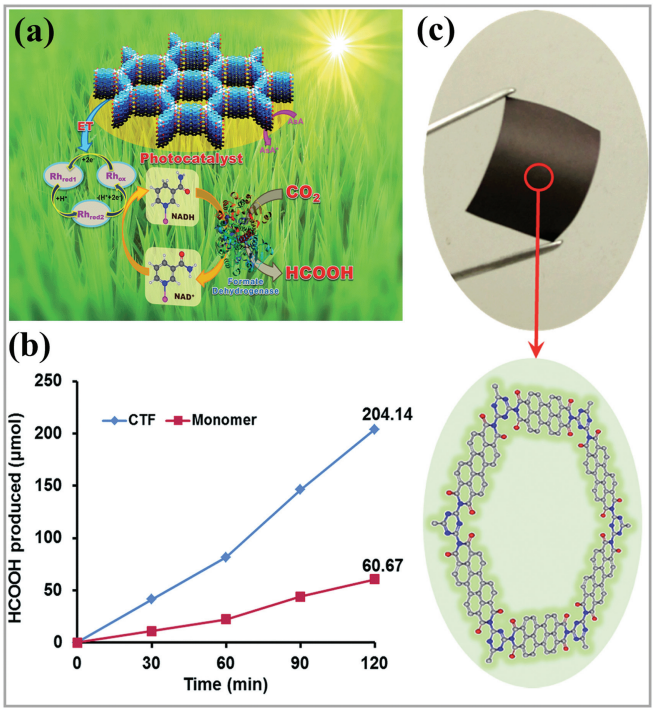

Fig. 17. (a) Schematic illustration of the CTF film photocatalyst-enzyme coupled system involved in the exclusive production of formic acid from CO_2. (b) Photocatalytic activities of the CTF and monomer for selective enzymatic production of formic acid from CO_2. (c) Photograph of the flexible film photocatalyst along with the detailed chemical structure of the CTF. Copied with permission [161]. Copyright 2016, the Royal Society of Chemistry.

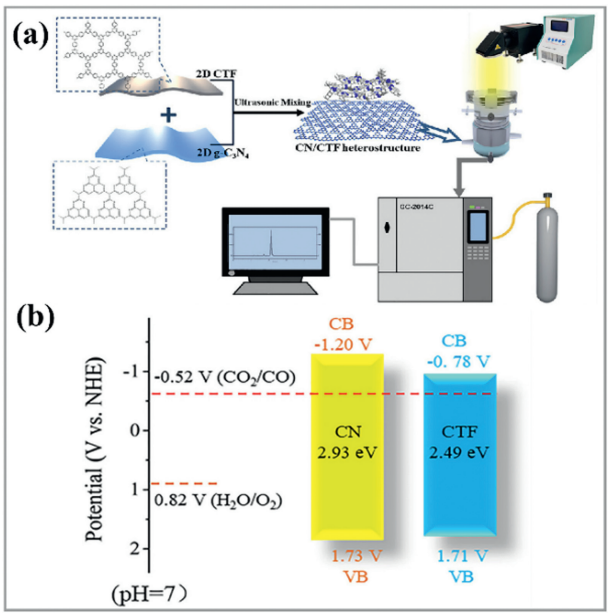

Fig. 18. (a) The synthesis and photocatalytic procedure of CN/CTF heterostructure. (b) Energy band structure of the as-synthesized CN/CTF heterostructure. Copied with permission [162]. Copyright 2018, the Royal Society of Chemistry.

metal atoms have shown remarkable activity and selectivity in this field, achieving the maximized atomic efficiency and diverse chemical activities of CTFs with possess large surface areas and tunable pore sizes.

Surface functionalization is another strategy to achieve high CO_2RR activity and product selectivity. Baeg *et al.* designed a photocatalyst/biocatalyst system utilizing perylene-based CTFs prepared through polycondensation between cyanuric chloride and perylene diimide that may provide an excellent platform to unify light harvesting capabilities of perylene with the desirable properties of CTFs for artificial photosynthesis (Fig. 17a) [161]. Upon irradiation, this system exclusively generates 9.3 μmol of HCOOH, with a formation rate of ~881.3 μmol h^{-1} g^{-1} in an elaborated buffer solution containing CTF, a coenzyme, a rhodium complex, a formate dehydrogenase enzyme, and ascorbic acid (Fig. 17b). The photograph of the flexible CTF film and the chemical structure is shown in Fig. 17c. Photoexcited electrons migrated to the photocatalyst/metal complex substrate, while photoexcited holes are captured by ascorbic acid to prevent rapid recombination. The metal complex undergoes reduction by excite electrons, coenzyme NADH, and formate dehydrogenase, ultimately resulting in the two-electron reduction of CO_2 to HCOOH. The polymeric structure, suitable band gap, and highly ordered π electron channel systems of the CTF film photocatalyst greatly facilitate charge carrier transport contribute to the excellent selectivity observed.

The positions of CBM and VBM of photocatalysts significantly influence the redox abilities of photo-generated electrons and holes during photocatalytic reactions. Zhu's work introduces aheterostructure of CTF and g-C_3N_4 in CO_2 photoreduction for the first time (Fig. 18a) [162]. The combined g-C_3N_4/CTF enhanced photocatalytic activity, achieving transform rates of CO_2 to CO reaching 151.1 μmol h^{-1} g^{-1} within 30 h. The optimal g-C_3N_4/CTF heterostructure efficiently separates charges and suppresses recombination under visible light irradiation, resulting in CO_2 photoreduction efficiency is 25.5 and 2.5 times higher than that of CTF and g-C_3N_4, respectively. The CBM potential of this heterostructure enables effective interfacial electrons transfer from g-C_3N_4 to CTF for thermodynamically favorable CO_2 reduction to CO. The VBM potentials of g-C_3N_4 and CTF, which are more positive than that of H_2O oxidization, allow the holes to oxidize H_2O to O_2 and H^+ (Fig. 18b). The stability of the g-C_3N_4/CTF heterostructure in photocatalytic systems is attributed to the crystal structure stability. Additionally, in the photocatalytic CO_2 reduction process, $[Co(bpy)_3]^{2+}$ acts as an electron harvesting agent from the semiconductor, activating CO_2 and breaking the C=O bond to selectively produce CO in synergy with g-C_3N_4/CTF. These outstanding features are expected to provide a new method for the fabrication of superior heterostructure photocatalysts by combining CTF with C_3N_4 to optimize the band structure and achieve higher product selectivity in this field.

Based on the above, several strategies can be employed to optimize CTFs for selective photocatalytic CO_2RR. These include the anchoring effect of single active sites, improvement of charge separation, fine-tuning of band structures, and enhancement of transfer efficiency through molecular-level structural design. Additionally, it is crucial to select an appropriate synthesis method to preserve the semiconductive property of the CTFs while also controlling the morphology and porosity for efficient photocatalytic applications. However, the synthesis of ordered and well-defined CTFs remains a significant challenge. The brief summary of the photocatalytic performances of the CTF-based photocatalysts in CO_2RR are listed in Table 3 [158-160,163-168].

3.3. Photocatalytic CO_2RR by cmp based catalysis

CMPs have attracted significant interest due to their porous structures and organic functionalities, which allow for various synthetic diversification. Since their first synthesis in 2007 by Cooper's group, a variety of CMPs, including thiophene-containing CMPs, light-emitting CMPs, soluble CMPs, core-shell CMPs, CMP films, comonomer-doped CMPs, and tetraphenylethylene-interweaving CMPs, have been developed for applications in gas adsorption,

Table 3
Summary of photocatalytic CO_2 reduction using CTF based photocatalysts.

Catalysts	Additive	Time (h)	Products (μmol g^{-1} h^{-1})[a]	Selectivity (%)	Ref.
Pt-SA/CTF-1	Pt/TEA	–	CO	100	[158]
Cu-SA/CTF	TEA	4	CH_4:32.6	98.3	[159]
Re-CTF-py	TEOA	10	CO:350	~100	[160]
α-Fe_2O_3@ Por-CTF	$Ru(bpy)_3Cl_2$/TEOA	–	CO:400	93	[163]
DA-CTF	2,2′-bpy/$CoCl_2$	2	CO:155	69	[164]
SnS_2/S-CTF	TEOA	4	CO:123.6	71	[165]
$ZnFe_2O_4$/FeP-CTFs	$Ru(bpy)_3^{2+}$	2	CO:178	–	[166]
TiO_2@CTF-Py	Coordinated Co^{2+}	4	CO:43.3	98.3	[167]
$CsPbBr_3$/CTF-1-Ni	Coordinated Ni^{2+}/EA	–	CO:86.5	95	[168]

[a] Maximum CO_2RR yield. TEOA: triethylamine; TEA: trimethylamine.

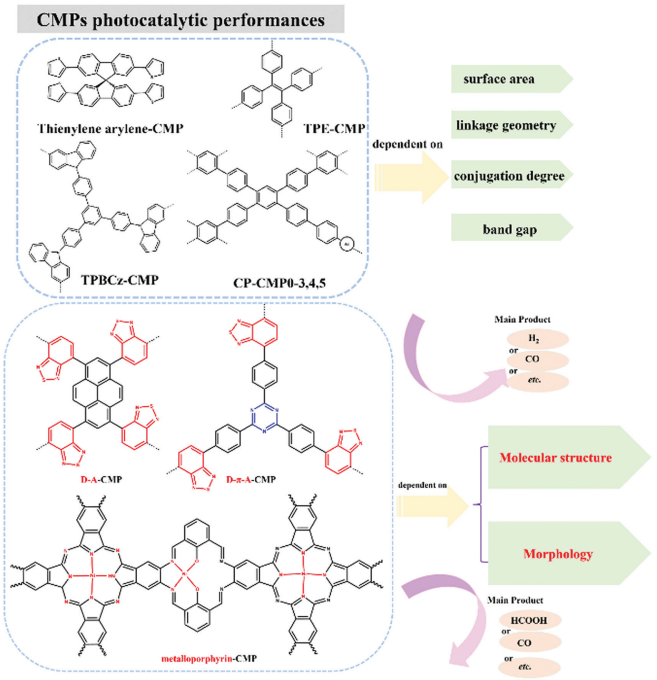

Fig. 19. Molecular based strategies to improve the photocatalytic performances of CMPs.

molecular separation, electronics, and catalysis. The photocatalytic performance of CMPs relies on factors such as surface area, linkage geometry, conjugation degree, and band gap. In recent years, various strategies have been proposed to improve photocatalytic performance of CMPs (Fig. 19).

One of the main strategies is to regulate the molecular structure of CMPs by adjusting synthesis methods, reaction conditions, and monomer types. This approach has been proven effective in enhancing their photocatalytic performance. Another strategy is to consider different donors and electron acceptor units, which can lead to the development of D–π–A CMP photocatalysts with expanded light absorption range [169]. Additionally, the morphology of CMP materials can also influence their photocatalytic performances. Surface modification with polar groups such as $-NO_2$ [170], arylamines [171], –OH [172], –COOH [173], $-SO_3H$ [174], and heterocyclic nitrogen atoms [175] can significantly increase the binding energy of CO_2 so as to improve CO_2 absorption ability.

By appropriate designing and constructing molecular building blocks, molecular-level precise control over chemical transformations catalyzed by CMPs can be achieved [176,177]. This has generated extensive interest in CMPs for CO_2 conversion. However, as far as we know, few examples have been reported on the use of CMPs as photocatalysts for CO_2 photoreduction in Table 4.

As discussed in the previous sections of this review, both COFs and CTFs exhibit intriguing optoelectronic properties, which can be further enhanced by utilizing different organic precursors and tuning their structures. One effective approach to achieve this is through molecular-based modification, where the optical characteristics of polymers can be easily adjusted by incorporating different organic moieties. For instance, Wang *et al.* explored the use of CMPs for CO_2 reduction and investigated the influence of their structure on catalytic efficiency [178]. By incorporating electron-withdrawing BT units into the triazine poly-network, the photocatalytic CO_2 reduction to CO was significantly enhanced, achieving CO formation rates of up to 18.2 μmol/h with a selectivity of 81.6%. The introduction of organic electron-withdrawing and electron-donating units in the polymer backbone, particularly based on triazine, promoted charge separation surface redox reactions, enabling stable photoconversion of CO_2 to CO under visible-light irradiation.

Furthermore, Xu's group designed a new 2D CMPs based on metalloporphyrin as the main structural and functional unit, with thiophene as the link moiety for CO_2 reduction [179]. They successfully modified the electronic properties of metalloporphyrin units by incorporating various metal atoms (Fe, Mg, Mn, and Cu) into CMP networks. Calculation results indicated that these CMPs possessed catalytic properties, high stability, and adjustable electronic structures, with Fe-modified thiophene-linked metalloporphyrin (Fe-TMP) exhibiting the highest catalytic activity for CO_2 reduction. The pathway for the H_3COH intermediate to CH_4 was also confirmed (Fig. 20a), with the adsorbed H_3COH^* being reduced to CH_3^* assisted by the adsorbed H atom. Finally, the formed CH_3^* species was further transferred to CH_4^* by another H atom. The thermodynamically preferred reduction process was the carboxyl pathway, resulting in methane as the final reduction product and formic acid as a side product.

To control the selectivity of photocatalysts, CO_2-philic monomers can be utilized in the construction of CMP networks to facilitate the efficient capture and highly selective conversion of CO_2. Recently, He's group reported the synthesis of two ferric porphyrin-based porous organic polymers semiconductors for visible light-driven CO_2RR to produce syngas with tunable CO/H_2 ratio (Fig. 20b) [180]. They found that the ferric porphyrin site was responsible for CO evolution, while the uncoordinated porphyrin unit played a role in H_2 formation, thus achieving selectivity control. The extended π-conjugation with a biphenyl linker in the polymer resulted in a lower conduction band potential, enabling the ferric porphyrin sites to capture electrons from the photosensitizer and produce more CO. By changing the linker from benzene to biphenyl, the ratio of CO/H_2 could be adjusted from 1:1 to 1:1.5, and under irradiation with 450 nm wavelengths, the ratio could reach 1:2. This demonstrated that modifying surface active sites was beneficial for improving product selectivity.

Another strategy involves providing multi-active sites to enhance catalytic efficiency and directly identify the activity of metal

Table 4
Summary of photocatalytic CO_2 reduction using CMPs.

Catalysts	Chemical structure	Additive	Products (μmol g^{-1} h^{-1})[a]	Selectivity (%)	Ref.
CMP-BT	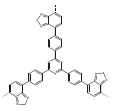	–	CO:1213.33	81.6	[178]
CMP-B	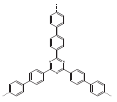	–	CO:266.67	66.7	[178]
CMP-Th	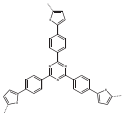	–	CO:666.67	76.9	[178]
POP2-Fe	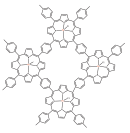	Ru complexes	CO:3043	50	[180]
Ni-Pc-NiPOP	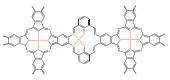	Ni complexes	CO:7770	96	[181]
BpyMP-1	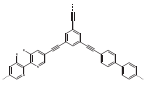	Cp*Rh	HCOOH:4300	–	[182]
PEosinY-1	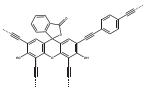	–	CO:33	92	[183]
PEosinY-2	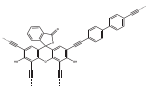	–	CO:26	86.7	[183]
PEosinY-3	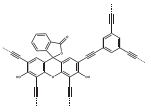	–	CO:12	28.6	[183]
N-CP-D	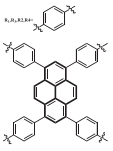	Co (II) bipyridine complexes	CO:2247	82	[184]

[a] Maximum CO_2RR yield. Cp*Ru: bipyridine-chelating macroligand.

centers. Zang's group designed and prepared a series of CMPs containing well-defined M–N_4 and M–N_2O_2 single-atom sites (Fig. 21a) [181]. The introduction of salphen unit with Ni–N_2O_2 catalytic centers into a phthalocyanine-based Ni–N_4 framework achieved remarkable CO generation ability (1942.5 μmol g^{-1} h^{-1}) with a high selectivity of 96% over H_2 in CO_2 photoreduction. Through control experiments and theoretical studies, the Ni–N_2O_2 moiety was found to be a more active site for CO_2RR compared to the traditional Ni–N_4 moiety. This can be attributed to the reduction of energy barriers, enhanced adsorption of reaction radicals *COOH by the M-N_2O_2 active sites, and improvement of the charge transportation (Figs. 21b and c). This study confirmed that molecular-based structural modification can easily tune the photoactivity and selectivity for photocatalytic CO_2RR.

Additionally, the presence of permanent porosity in these materials allows for facile diffusion of substrate, while π-conjugation throughout the CMP network facilitates charge migration to reaction sites [182,183]. Inspired by the intermolecular π–π stacking structure of Co (II) bipyridine complex cocatalyst, Ye and coworkers constructed a series of novel CMPs (Fig. 22a) through Sonogashira and Suzuki coupling methods, with or without alkynyl bridges and pyrene comonomers possessing two or four functional end groups, resulting in linear or crosslinked polymers [184]. Combined with simulation and experimental results, they found that the presence of alkyne facilitated intramolecular electron transfer, leading to lower local electron density and thus poor intermolecular electron transfer between photocatalysts and cocatalysts (Fig. 22b). CO_2 photoreduction experiments supported their findings, demonstrating higher CO production rates (11.37 and 4.03 μmol/h) for samples without alkynyl bridges. Alkynyl-containing photocatalysts only generated a moderate amount of CO (0.5 μmol/h).

4. Summary and perspective

In this review, we provide a comprehensive summary of recent advancements in molecular-based design of PPs for photocatalytic CO_2 reduction. Molecular design plays a pivotal role in achieving desired properties of polymers. For instance, tethering an

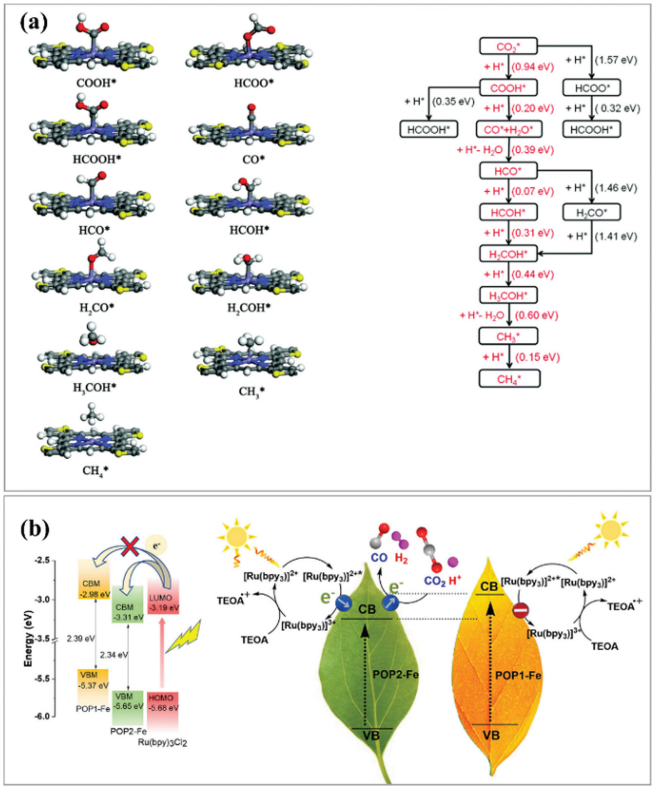

Fig. 20. The mechanism of CO_2RR of metalloporphyrin based CMPs. (a) The optimized structures of various intermediate species adsorbed on the Fe-TMP substrate and the overall pathway of CO_2 reduction and each elemental step's activation barriers. Copied with permission [179]. Copyright 2018, the Royal Society of Chemistry. (b) The energy-level diagram and proposed mechanism for photocatalytic CO_2RR of POPn-Fe. Copied with permission [180]. Copyright 2021, American Chemical Society.

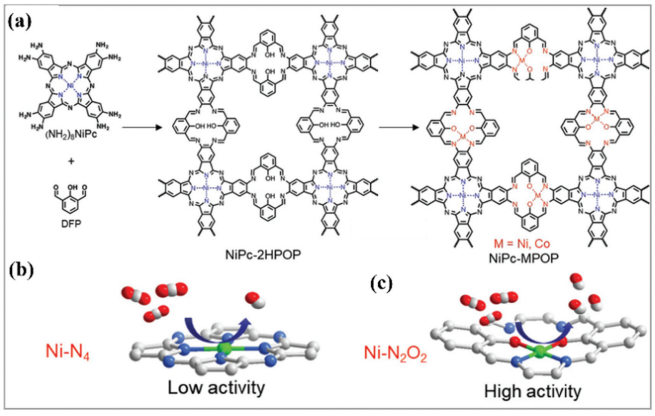

Fig. 21. (a) The structure of NiPc–MPOP and the high CO_2 reduction activity of Ni–N_2O_2 species compared to that of Ni–N_4. (b, c) The high CO_2 reduction activity of Ni–N_2O_2 species compared to that of Ni–N_4. Copied with permission [181]. Copyright 2021, Wiley-VCH.

antenna molecule can improve visible light absorption, constructing Z-scheme photocatalyst system can decrease the recombination of charge carriers, and deposition of highly dispersed single active site can provide more active sites. The influence of atom manufacturing on heterogeneous photocatalysts is explored, highlighting the importance of active sites, light absorption capabilities, and the transportation of photogenerated carriers. Various molecular manufacturing approaches, such as single active site, anchoring metal molecular complexes, and metal-semiconductor systems, are discussed for their potential to improve performance and product

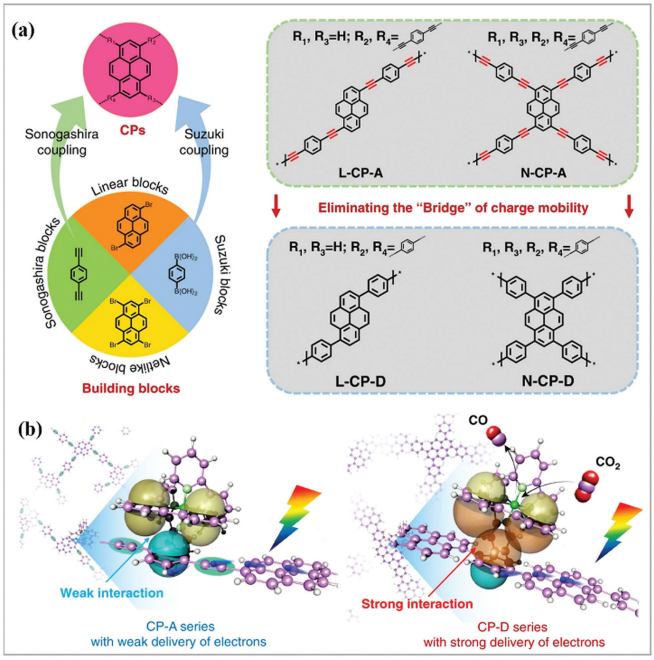

Fig. 22. (a) Illustration of synthesis and the strategy of eliminating the charge-transfer bridge. (b) Proposed process of electron transfer over the CP-A series and CP-D series for the CO_2 photoreduction reaction. Copied with permission [184]. Copyright 2020, Springer Nature.

selectivity in photocatalytic CO_2RR. Molecular engineering of PPs enables favorable electronic structure regulation of active sites, affecting CO_2 adsorption and activation behaviors, thereby enhancing CO_2 conversion efficiency and product selectivity.

While these PPs have proven to be promising photocatalysts, further efforts are required to compete with traditional photocatalysts and address some key challenges in the future. While catalyst design represents a crucial step and has made significant progress, the understanding of the reaction mechanism and pathways involved in photocatalytic CO_2 reduction remains in its nascent stages. To achieving high activity and product selectivity in CO_2 reduction photocatalysts, further exploration and optimization of various factors are necessary. These factors include band structure, charge carrier separation, reactant adsorption/activation, surface reaction sites, and intermediate adsorption/desorption processes. Challenges and obstacles persist in the design, fabrication, and application of modified photocatalysts. It is imperative to focus on developing highly efficient methods for scalable production of controllable molecular-based porous polymers. Additionally, a deeper comprehension of the structure-activity relationship between molecular-based photocatalysts and their performance is crucial. Exploring the effects of surface or interface-engineered atoms, rather than bulk atoms, on CO_2 reduction may offer valuable insights.

Regarding the PPs we mentioned in this review, many issues need to be resolved. For COF-based PPs, research can focus on developing core-shell structures to enhance charge separation at intimate interfaces between the COF and supports. The design of COFs with donor–acceptor (D–A) structures can also facilitate intramolecular charge transfer to achieve efficient photocatalytic CO_2 reduction. Compared to COFs, CTFs have a limited number of structures that are well-defined and crystalline, which has posed challenges to conducting in-depth studies on structure-activity relationships. Therefore, there is a pressing need for advanced development in CTF synthesis to address this limitation. Despite their potential, CMPs still face challenges in competing with other pho-

tocatalysts. It is crucial to develop suitable synthetic strategies to incorporate photocatalytically active components into CMP networks for more complex reactions. Moreover, efforts should be made to enhance the crystallinity of CMPs or design novel structures that facilitate efficient charge transfer and minimize photoexcited carriers recombination.

In conclusion, the molecular-based strategy shows promising potential for creating highly efficient photocatalysts for CO_2RR. Anticipated breakthroughs in molecular-based photocatalysts are expected in the near future, and are poised to greatly improve the selective photocatalytic conversion of CO_2.

Declaration of competing interest

The authors declare that they have no known competing financial interests or personal relationships that could have appeared to influence the work reported in this paper.

Acknowledgment

We appreciate the National Natural Science Foundation of China (No. 22005154) for financial support.

References

[1] M. Meinshausen, N. Meinshausen, W. Hare, et al., Nature 458 (2009) 1158–1162.
[2] T.R. Karl, K.E. Trenberth, Science 302 (2003) 1719–1723.
[3] C. Zhou, J. Shi, W. Zhou, et al., ACS Catal. 10 (2020) 302–310.
[4] Q. Guo, S.G. Xia, X.B. Li, et al., Chem. Commun. 56 (2020) 7849.
[5] W. Zhou, K. Cheng, J. Kang, et al., Chem. Soc. Rev. 48 (2019) 3193–3228.
[6] L. Lu, X.F. Sun, J. Ma, et al., Angew. Chem. Int. Ed. 57 (2018) 14149–14153.
[7] X. He, Y. Cao, X.D. Lang, et al., ChemSusChem 11 (2018) 3382–3387.
[8] J. Artz, T.E. Müller, K. Thenert, et al., Chem. Rev. 118 (2018) 434–504.
[9] K. Chen, J. Xiao, T. Hisatomi, et al., Chem. Sci. 14 (2023) 9248–9257.
[10] G. Wang, C.T. He, R. Huang, et al., J. Am. Chem. Soc. 142 (2020) 19339–19345.
[11] Y.N. Gong, J.H. Mei, W.J. Shi, et al., Angew. Chem. Int. Ed. 63 (2024) e202318735.
[12] J.H. Zhang, Y.N. Gong, H.J. Wang, et al., Proc. Natl. Acad. Sci. U. S. A. 119 (2022) e2118278119.
[13] Q. Zhang, S. Gao, Y. Guo, et al., Nat. Commun. 14 (2023) 1147.
[14] J. Zhang, Y. Wang, H. Wang, D. Zhong, T. Lu, Chin. Chem. Lett. 33 (2022) 2065–2068.
[15] M.T. Ming, Y.C. Wang, W.X. Tao, et al., Green Chem. 25 (2023) 6207–6211.
[16] H. Lv, P. Li, X. Li, et al., Chem. Eng. J. 451 (2023) 138745.
[17] J.W. Liu, C.Y. Chen, K. Zhang, L. Zhang, Chin. Chem. Lett. 32 (2021) 649–659.
[18] N. Elgrishi, M.B. Chambers, X. Wang, M. Fontecave, Chem. Soc. Rev. 46 (2017) 761–796.
[19] M. Ding, R.W. Flaig, H.L. Jiang, O.M. Yaghi, Chem. Soc. Rev. 48 (2019) 2783–2828.
[20] H. Rao, C. Lim, J. Bonin, G.M. Miyake, M. Robert, J. Am. Chem. Soc. 140 (2018) 17830–17834.
[21] A. Savateev, M. Antonietti, ACS Catal. 8 (2018) 9790–9808.
[22] X.B. Li, C.H. Tung, L.Z. Wu, Nat. Rev. Chem. 2 (2018) 160–173.
[23] A.G. Slater, A.I. Cooper, Science 348 (2015) aaa8075.
[24] C. Cometto, R. Kuriki, L. Chen, et al., J. Am. Chem. Soc. 140 (2018) 7437–7440.
[25] Y. Li, S. Zhang, W. Cheng, et al., Adv. Mater. 34 (2022) 2105204.
[26] H. Kim, D. Shin, W. Yang, et al., J. Am. Chem. Soc. 143 (2021) 925–933.
[27] A. Savateev, I. Ghosh, B. König, M. Antonietti, Angew. Chem. Int. Ed. 57 (2018) 15936–15947.
[28] W.J. Wang, K.H. Chen, Z.W. Yang, B.W. Peng, L.N. He, J. Mater. Chem. A 9 (2021) 16699–16705.
[29] X. Wang, Y. Pan, H. Ning, et al., Appl. Catal. B 266 (2020) 118630.
[30] Y. Li, S. Wang, X.S. Wang, et al., J. Am. Chem. Soc. 142 (2020) 19259–19267.
[31] Y.N. Gong, L. Jiao, Y. Qian, et al., Angew. Chem. Int. Ed. 59 (2020) 2705–2709.
[32] A. Guan, Z. Chen, Y. Quan, et al., ACS Energy Lett. 5 (2020) 1044–1053.
[33] Y. Cai, J. Fu, Y. Zhou, et al., Nat. Commun. 12 (2021) 586.
[34] D. Gao, T. Liu, G. Wang, X. Bao, ACS Energy Lett. 6 (2021) 713–727.
[35] X. Cui, W. Li, P. Ryabchuk, K. Junge, M. Beller, Nat. Catal. 1 (2018) 385–397.
[36] R. Lang, T. Li, D. Matsumura, et al., Angew. Chem. Int. Ed. 55 (2016) 16054–16058.
[37] S. Lin, C.S. Diercks, Y.B. Zhang, et al., Science 349 (2015) 1208–1213.
[38] G. Huang, Q. Niu, J. Zhang, et al., Chem. Eng. J. 427 (2022) 131018.
[39] J.H. Kou, C.H. Lu, J. Wang, et al., Chem. Rev. 117 (2017) 1445–1514.
[40] L. Rademacher, T. Beglau, B. Ali, et al., J. Mater. Chem. A 12 (2024) 2093–2109.
[41] Y. Liang, X. Wu, X. Liu, C. Li, S. Liu, Appl. Catal. B 304 (2022) 120978.
[42] J. Ran, M. Jaroniec, S.Z. Qiao, Adv. Mater. 30 (2018) 1704649.
[43] K. Li, B. Peng, T. Peng, ACS Catal. 6 (2016) 7485–7527.
[44] H.L. Wu, X.B. Li, C.H. Tung, L.Z. Wu, Adv. Mater. 31 (2019) 1900709.
[45] S. Kramer, N.R. Bennedsen, S. Kegnæs, ACS Catal. 8 (2018) 6961–6982.
[46] P. Kaur, J.T. Hupp, S.T. Nguyen, ACS Catal. 1 (2011) 819–835.
[47] C. Qian, W. Zhou, J. Qiao, et al., J. Am. Chem. Soc. 142 (2020) 18138–18149.
[48] J.Q. Dong, X. Han, Y. Liu, H.Y. Li, Y. Cui, Angew. Chem. Int. Ed. 59 (2020) 13722–13733.
[49] B. Han, X. Ou, Z. Zhong, et al., Small 16 (2020) 2002985.
[50] C. Dai, B. Liu, Energy Environ. Sci. 13 (2020) 24–52.
[51] X. Chen, S. Shen, L. Guo, S.S. Mao, Chem. Rev. 110 (2010) 6503–6570.
[52] X. Liu, S. Inagaki, J. Gong, Angew. Chem. Int. Ed. 55 (2016) 14924–14950.
[53] C. Wang, Z. Sun, Y. Zheng, Y.H. Hu, J. Mater. Chem. A 7 (2019) 865–887.
[54] X. Wang, S. Blechert, M. Antonietti, ACS Catal. 2 (2012) 1596–1606.
[55] Y. Zheng, L. Lin, B. Wang, X. Wang, Angew. Chem. Int. Ed. 54 (2015) 12868–12884.
[56] C. Chen, W. Ma, J. Zhao, Chem. Soc. Rev. 39 (2010) 4206–4219.
[57] D.D. Zhu, J.L. Liu, S.Z. Qiao, Adv. Mater. 28 (2016) 3423.
[58] S. Zhang, S. Wang, L. Guo, et al., J. Mater. Chem. C 8 (2020) 192–200.
[59] H.P. Liang, A. Acharjya, D.A. Anito, et al., ACS Catal. 9 (2019) 3959–3968.
[60] Y. Chen, G. Ji, S. Guo, et al., Green Chem. 19 (2017) 5777–5781.
[61] L. Zhang, Z.J. Zhao, J. Gong, Angew. Chem. Int. Ed. 56 (2017) 11326–11353.
[62] X.F. Yang, A. Wang, B. Qiao, et al., Acc. Chem. Res. 46 (2013) 1740–1748.
[63] J.L. White, M.F. Baruch, J.E. Pander III, et al., Chem. Rev. 115 (2015) 12888–12935.
[64] M.R. Hoffmann, S.T. Martin, W. Choi, D.W. Bahnemann, Chem. Rev. 95 (1995) 69–96.
[65] A.L. Linsebigler, G. Lu, J.T. Yates, Chem. Rev. 95 (1995) 735–758.
[66] S. Sorcar, Y. Hwang, C.A. Grimes, Mater. Today 20 (2017) 507–515.
[67] P.V. Kamat, J. Phys. Chem. Lett. 3 (2012) 663–672.
[68] M.A. Henderson, Surf. Sci. Rep. 66 (2011) 185–297.
[69] A. Fujishima, X. Zhang, D.A. Tryk, Surf. Sci. Rep. 63 (2008) 515–582.
[70] S.H. Szczepankiewicz, A.J. Colussi, M.R. Hoffmann, J. Phys. Chem. B 104 (2000) 9842–9850.
[71] D.M. Adams, L. Brus, C.E.D. Chidsey, et al., J. Phys. Chem. B 107 (2003) 6668–6697.
[72] M. Jakob, H. Levanon, P.V. Kamat, Nano Lett. 3 (2003) 353–358.
[73] S. Kim, S.J. Hwang, W. Choi, J. Phys. Chem. B 109 (2005) 24260–24267.
[74] J.T. DuBose, P.V. Kamat, Chem. Rev. 122 (2022) 12475–12494.
[75] X. Chang, T. Wang, J. Gong, Energy Environ. Sci. 9 (2016) 2177–2196.
[76] A. Behera, A.K. Kar, R. Srivastava, Mater. Horiz. 9 (2022) 607–639.
[77] T. Oshima, T. Ichibha, K. Qin, et al., Angew. Chem. Int. Ed. 57 (2018) 8154–8158.
[78] S.N. Habisreutinger, L. Schmidt-Mende, J.K. Stolarczyk, Angew. Chem. Int. Ed. 52 (2013) 7372–7408.
[79] A. Wang, J. Li, T. Zhang, Nat. Rev. Chem. 2 (2018) 65–81.
[80] B. Qiao, A. Wang, X. Yang, et al., Nat. Chem. 3 (2011) 634–641.
[81] L.H. Shao, A.X. Huang, X.C. Yan, et al., J. Colloid Interface Sci. 633 (2023) 233–242.
[82] J. Fu, B. Zhu, C. Jiang, et al., Small 13 (2017) 1603938.
[83] B.H. Lee, S. Park, M. Kim, et al., Nat. Mater. 18 (2019) 620–626.
[84] C. Gao, J. Low, R. Long, et al., Chem. Rev. 120 (2020) 12175–12216.
[85] J.C. Liu, Y. Tang, Y.G. Wang, T. Zhang, J. Li, Natl. Sci. Rev. 5 (2018) 638–641.
[86] J. Li, Q. Guan, H. Wu, et al., J. Am. Chem. Soc. 141 (2019) 14515–14519.
[87] Y. Zhang, B. Xia, J. Ran, K. Davey, S.Z. Qiao, Adv. Energy Mater. 10 (2020) 1903879.
[88] A.P. Côté, A.I. Benin, N.W. Ockwig, et al., Science 310 (2005) 1166–1170.
[89] H. Wang, H. Wang, Z. Wang, et al., Chem. Soc. Rev. 49 (2020) 4135–4165.
[90] K.K. Niu, T.X. Luan, J. Cui, et al., ACS Catal. 14 (2024) 2631–2641.
[91] C.Y. Lin, D.T. Zhang, Z.H. Zhao, Z.H. Xia, Adv. Mater. 30 (2018) 1703646.
[92] P. Pachfule, A. Acharjya, J. Roeser, et al., J. Am. Chem. Soc. 140 (2018) 1423–1427.
[93] T. Sick, A.G. Hufnagel, J. Kampmann, et al., J. Am. Chem. Soc. 140 (2018) 2085–2092.
[94] J.D. Xiao, H.L. Jiang, Acc. Chem. Res. 52 (2019) 356–366.
[95] X. Liu, X. Ding, T. Zheng, et al., ACS Appl. Mater. Interfaces 16 (2024) 4741–4750.
[96] Y. Fu, X. Zhu, L. Huang, et al., Appl. Catal. B 239 (2018) 46.
[97] F. Chen, H. Huang, L. Guo, Y. Zhang, T. Ma, Angew. Chem. Int. Ed. 58 (2019) 10061–10073.
[98] J. Fu, K. Jiang, X. Qiu, J. Yu, M. Liu, Mater. Today 32 (2020) 222–243.
[99] S. Xu, E.A. Carter, Chem. Rev. 119 (2019) 6631–6669.
[100] Y. Fang, X. Wang, Chem. Commun. 54 (2018) 5674–5687.
[101] E. Jin, M. Asada, Q. Xu, et al., Science 357 (2017) 673–676.
[102] R. Chen, J.L. Shi, Y. Ma, et al., Angew. Chem. Int. Ed. 58 (2019) 6430–6434.
[103] S. Yang, W. Hu, X. Zhang, et al., J. Am. Chem. Soc. 140 (2018) 14614–14618.
[104] Z. Fu, X. Wang, A.M. Gardner, et al., Chem. Sci. 11 (2020) 543–550.
[105] W. Zhong, R. Sa, L. Li, et al., J. Am. Chem. Soc. 141 (2019) 7615–7621.
[106] D.L. Meng, M.D. Zhang, D.H. Si, et al., Angew. Chem. Int. Ed. 60 (2021) 25485–25492.
[107] H.B. Huang, Z.B. Fang, R. Wang, et al., Small 18 (2022) e2200407.
[108] P.X. Li, X.Y. Yan, X.M. Song, et al., ACS Sustain. Chem. Eng. 9 (2021) 2319–2325.
[109] H. Zhao, X. Yang, R. Xu, et al., J. Mater. Chem. A 6 (2018) 20152–20160.
[110] M. Lu, J. Liu, Q. Li, et al., Angew. Chem. Int. Ed. 58 (2019) 12392–12397.
[111] X. Wang, X. Ding, T. Wang, et al., ACS Appl. Mater. Interfaces 14 (2022) 41122–41130.
[112] J. Tang, Z. Liang, H. Qin, et al., Angew. Chem. Int. Ed. 62 (2023) e202214449.
[113] M. Zhang, M. Lu, Z.L. Lang, et al., Angew. Chem. Int. Ed. 59 (2020) 6500–6506.

[114] D. Wang, X. Li, L.L. Zheng, et al., Nanoscale 10 (2018) 19509–19516.
[115] D. Wang, H. Zeng, X. Xiong, et al., Sci. Bull. 65 (2020) 113–122.
[116] R. Gao, J. Bai, R. Shen, et al., J. Mater. Sci. Technol. 137 (2023) 223–231.
[117] Y. Chen, D. Yang, Y. Gao, et al., Research 2021 (2021) 9798564.
[118] Y. Wang, Z. Hu, W. Wang, et al., Chem. Sci. 12 (2021) 16065–16073.
[119] Y. Feng, J. Li, S. Ye, S. Gao, R. Cao, Sustain. Energy Fuels 6 (2022) 5089–5099.
[120] C.C. Li, M.Y. Gao, X.J. Sun, et al., Appl. Catal. B 266 (2020) 118586.
[121] L. Liu, J. Zhang, X. Tan, et al., Nano Res. 13 (2020) 983–988.
[122] M. Zhang, J.N. Chang, Y.F. Chen, et al., Adv. Mater. 23 (2021) 2105002.
[123] P. Dong, A. Zhang, T. Cheng, et al., Chin. J. Catal. 43 (2022) 2592–2605.
[124] C. Lin, C. Han, L. Gong, et al., Catal. Sci. Technol. 11 (2021) 2616–2621.
[125] W. Han, L.H. Shao, X.J. Sun, et al., Appl. Catal. B 317 (2022) 121710.
[126] G. Yuan, L. Tan, P. Wang, et al., Mater. Lett. 325 (2022) 132863.
[127] Z. Han, R. Kortlever, H.Y. Chen, J.C. Peters, T. Agapie, ACS Cent. Sci. 3 (2017) 853–859.
[128] S. Ou, M. Zhou, W. Chen, Y. Zhang, Y. Liu, ChemSusChem 15 (2022) e202200184.
[129] Q. Sun, B. Aguila, J. Perman, N. Nguyen, S. Ma, J. Am. Chem. Soc. 138 (2016) 15790–15796.
[130] J. Thote, H.B. Aiyappa, A. Deshpande, et al., Chem. Eur. J. 20 (2014) 15961–15965.
[131] B.P. Biswal, H.A. Vignolo-González, T. Banerjee, et al., J. Am. Chem. Soc. 141 (2019) 11082–11092.
[132] T. Banerjee, F. Haase, G. Savasci, et al., J. Am. Chem. Soc. 139 (2017) 16228–16234.
[133] Y. Liu, Y. He, Anal. Chem. 95 (2023) 14440–14446.
[134] H. Zhong, R. Sa, H. Lv, et al., Adv. Funct. Mater. 30 (2020) 2002654.
[135] V.N. Gopalakrishnan, D.T. Nguyen, J. Becerra, et al., ACS Appl. Energy Mater. 4 (2021) 6005–6014.
[136] J. Wang, Y. Yu, J. Cui, et al., Appl Catal. B 301 (2022) 120814.
[137] H. Lin, Y. Liu, Z. Wang, et al., Angew. Chem. Int. Ed. 61 (2022) e202214142.
[138] W. Shi, X. Guo, C. Cui, et al., Appl. Catal. B 243 (2019) 236.
[139] Y. Fu, D. Sun, Y. Chen, et al., Angew. Chem. Int. Ed. 51 (2012) 3364–3367.
[140] D. Sun, Y. Fu, W. Liu, et al., Chem. Eur. J. 19 (2013) 14279–14285.
[141] D. Sun, W. Liu, Y. Fu, et al., Chem. Eur. J. 20 (2014) 4780–4788.
[142] S. Zhang, S. Wang, L. Guo, et al., J. Mater. Chem. C 8 (2020) 192–200.
[143] B. Zhu, L. Zhang, D. Xu, B. Cheng, J. Yu, J. CO_2 Util. 21 (2017) 327–335.
[144] Z.J. Li, D.H. Wang, Y.E. Wu, Y.D. Li, Natl. Sci. Rev. 5 (2018) 673–689.
[145] M.Z. Ma, Z.A. Huang, D.E. Doronkin, et al., Appl. Catal. B 300 (2022) 120695.
[146] K. Qi, M. Chhowalla, D. Voiry, Mater. Today 40 (2020) 173.
[147] J. Liang, Q. Song, J. Wu, et al., ACS Nano 16 (2022) 4152–4161.
[148] Q. Jiang, L. Sun, J. Bi, et al., ChemSusChem 11 (2018) 1108–1113.
[149] T. Jadhav, Y. Fang, W. Patterson, et al., Angew. Chem. Int. Ed. 58 (2019) 13753–13757.
[150] P. Puthiaraj, Y.R. Lee, S. Zhang, W.S. Ahn, J. Mater. Chem. A 4 (2016) 16288–16311.
[151] J.S.M. Lee, A.I. Cooper, Chem. Rev. 120 (2020) 2171–2214.
[152] P. Kuhn, M. Antonietti, A. Thomas, Angew. Chem. Int. Ed. 47 (2008) 3450–3453.
[153] H.B. Yang, S.F. Hung, S. Liu, et al., Nat. Energy 3 (2018) 140–147.
[154] X.M. Hu, H.H. Hval, E.T. Bjerglund, et al., ACS Catal. 8 (2018) 6255–6264.
[155] C. Costentin, S. Drouet, M. Robert, J.M. Savéant, Science 338 (2012) 90–94.
[156] J. Shen, R. Kortlever, R. Kas, et al., Nat. Commun. 6 (2015) 8177.
[157] X. Zhu, C. Tian, G.M. Veith, et al., J. Am. Chem. Soc. 138 (2016) 11497–11500.
[158] G. Huang, Q. Niu, J. Zhang, et al., Chem. Eng. J. 427 (2022) 131018.
[159] G. Huang, Q. Niu, Y. He, et al., Nano Res. 15 (2022) 8001–8009.
[160] R. Xu, X.S. Wang, H. Zhao, et al., Catal. Sci. Technol. 8 (2018) 2224–2230.
[161] R.K. Yadav, A. Kumar, N.J. Park, K.J. Kong, J.O.A. Baeg, J. Mater. Chem. A 4 (2016) 9413–9418.
[162] J. He, X. Wang, S. Jin, Z.Q. Liu, M. Zhu, Chin. J. Catal. 43 (2022) 1306–1315.
[163] R. Luo, M. Chen, F. Zhou, et al., J. Mater. Chem. A 9 (2021) 25731–25749.
[164] J. Bi, B. Xu, L. Sun, et al., ChemSusChem 12 (2019) 4493–4499.
[165] S. Guo, P. Yang, Y. Zhao, et al., ChemSusChem 13 (2020) 6278–6283.
[166] Y.L. Yan, Q.J. Fang, J.k. Pan, et al., Chem. Eng. J. 408 (2021) 127358.
[167] P. Gotico, B. Boitrel, R. Guillot, et al., Angew. Chem. Int. Ed. 58 (2019) 4504–4509.
[168] Q. Wang, J. Wang, J.C. Wang, et al., ChemSusChem 14 (2021) 1131–1139.
[169] R.S. Sprick, J.X. Jiang, B. Bonillo, et al., J. Am. Chem. Soc. 137 (2015) 3265–3270.
[170] R. Banerjee, H. Furukawa, D. Britt, et al., J. Am. Chem. Soc. 131 (2009) 3875-3270.
[171] R. Vaidhyanathan, S.S. Iremonger, G.K.H. Shimizu, et al., Science 330 (2010) 650–653.
[172] W. Lu, D. Yuan, J. Sculley, et al., J. Am. Chem. Soc. 133 (2011) 18126–18129.
[173] L.H. Xie, M.P. Suh, Chem. Eur. J. 19 (2013) 11590–11597.
[174] L. Qin, G.J. Xu, C. Yao, Y.H. Xu, Chem. Commun. 52 (2016) 12602–12605.
[175] A. Yassin, M. Trunk, F. Czerny, et al., Adv. Funct. Mater. 27 (2017) 1700233.
[176] D.S. Amaraseela, N.M. Sarih, S. Habibu, Energy Adv. 2 (2023) 1127–1133.
[177] J. Weber, A. Thomas, J. Am. Chem. Soc. 130 (2008) 6334–6335.
[178] C.A. Trickett, A. Helal, B.A. Almaythalony, et al., Nat. Rev. Mater. 2 (2017) 201745.
[179] C. Chen, C. Tang, W. Xu, Y. Li, L. Xu, Phys. Chem. Chem. Phys. 20 (2018) 9536–9542.
[180] X. Yao, K. Chen, L.Q. Qiu, Z.W. Yang, L.N. He, Chem. Mater. 33 (2021) 8863–8872.
[181] X.Y. Dong, Y.N. Si, Q.Y. Wang, S. Wang, S.Q. Zang, Adv. Mater. 33 (2021) 2101568.
[182] Y. Xie, T.T. Wang, X.H. Liu, K. Zou, W.Q. Deng, Nat. Commun. 4 (2013) 1960.
[183] X. Yu, Z. Yang, B. Qiu, et al., Angew. Chem. Int. Ed. 58 (2019) 632–636.
[184] S. Wang, X. Hai, X. Ding, et al., Nat. Commun. 11 (2020) 1149.